Journal of Colloid and Interface Science 498 (2017) 292–297

Contents lists available at ScienceDirect

Journal of Colloid and Interface Science

journal homepage: www.elsevier.com/locate/jcis

# ZnO nanorods array based field-effect transistor biosensor for phosphate detection

Rafiq Ahmad, Min-Sang Ahn, Yoon-Bong Hahn *

*School of Semiconductor and Chemical Engineering, Nanomaterials Processing Research Center, Chonbuk National University, 567 Baekjedaero, Deokjin-gu, Jeonju-si, Jeollabuk-do 54896, Republic of Korea*

## HIGHLIGHTS

- Growth of ZnO nanorods on substrate via low-temperature aqueous route.
- Functionalization of ZnO NRs with pyruvate oxidase to detect phosphate.
- Vertically grown ZnO NRs provides high specific surface area for enhanced enzyme immobilization.
- As-fabricated FET biosensor showed high sensitivity in a wide-linear range.

## GRAPHICAL ABSTRACT

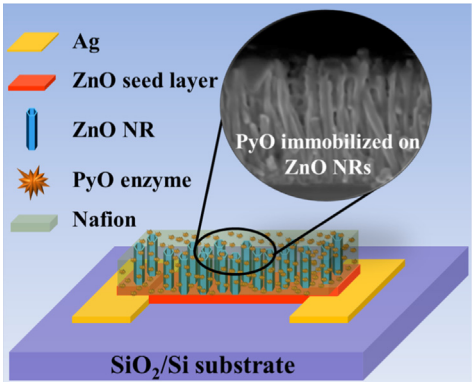


## ARTICLE INFO

*Article history:*
Received 31 January 2017
Revised 8 March 2017
Accepted 15 March 2017
Available online 18 March 2017

*Keywords:*
ZnO nanorods
Field-effect transistor
Phosphate biosensor
Pyruvate oxidase
High sensitivity

## ABSTRACT

A promising field-effect transistor (FET) biosensor has been fabricated based on pyruvate oxidase (PyO) functionalized ZnO nanorods (ZnO NRs) array grown on seeded $SiO_2$/Si substrate. The direct and vertically grown ZnO NRs on the seeded $SiO_2$/Si substrate offers high surface area for enhanced PyO immobilization, which further helps to detect phosphate with higher specificity. Under optimum conditions, the fabricated FET biosensor provided a convenient method for phosphate detection with high sensitivity (80.57 μA $mM^{-1}$ $cm^{-2}$) in a wide-linear range (0.1 μM–7.0 mM). Additionally, it also showed very low effect of electroactive species, stability and good reproducibility. Encouraging results suggest that this approach presents a promising method to be used for field measurements to detect phosphate.



## 1. Introduction

Phosphate is one of the well-established essential nutrients needed for critical biological reactions, living organisms, and water quality managements [1]. Importantly, phosphate is used to preserve meat, soft cheeses production, as melting salts component, in soft drinks, and in different powdered products [2]. Phosphorous are taken in the form of phosphates by our bodies from different foods that is critically important for health. Institute of Medicine (The food and nutrition board, 1997) has recommended dietary allowance of 700–1250 mg/day phosphorus for healthy human [3]. This level of consumption helps to maintain the serum phosphorus concentrations within the normal physiological range of 0.80–1.45 mM (2.5–4.5 mg/dL) [3]. Hence, it is essential to take regular adequate intake of phosphorus in our diets, as phosphate

* Corresponding author.
*E-mail address:* ybhahn@chonbuk.ac.kr (Y.-B. Hahn).

http://dx.doi.org/10.1016/j.jcis.2017.03.069
0021-9797/

is used in the production of proteins, bone, cell membrane, and other biomolecules [4]. However, excessive uptake could damage blood vessels and as a result it also induces the aging processes [2]. As compared to natural food, phosphate contents are much higher in industrially processed food [5]. Among all other phosphate sources, water supplies have larger quantities of phosphate, which is mainly from industrial discharge, laundering, and commercial cleaning fluids. Therefore, phosphate monitoring is needed in water to avoid the drinking of high content phosphate water.

Among various methods used for the analysis of phosphate in natural waters, color-forming reagents based spectrophotometric methods have been the most promising, selective and sensitive which have formed the basis of many *in situ* analyzers for environmental analysis [6–18]. However, all spectrophotometric based methods are time, cost and labor-intensive, and also during transfer and storage it carries risks of sample contamination and degradation. Therefore, to overcome these shortcomings during phosphate monitoring different groups have proposed/developed instrumentation for near continuous detection in aquatic environments [19–21]. But, their large physical size, excessive power and reagent consumptions limit its ways for deployment. Thus, development of a reliable method for analysis of phosphate in diverse foods containing phosphate additives and water is highly desirable.

There is demand of sensors that not only accurately and reliably determine pollutants and but also have the ability of continuous monitoring in wastewater. It would help for the preservation of high quality water bodies and provide most reliable and economical environmental protection. Attempts have been made to develop phosphate sensors to replace the current colorimetric based sensors used in laboratory-based assays/field-deployed instruments [22]. In recent year's biosensor utilizing different nanomaterials have attracted interest of researchers to fabricate cost-effective, simple, and selective phosphate biosensors [23–28]. Recently, Cinti et al. fabricated reagent-free paper-based screen-printed electrochemical based phosphate sensor to detect phosphate ions [24]. Fadhel et al. prepared gold nanoparticles capped with a cetyltrimethylammonium bromide (Au NPs-CTAB) to fabricate phosphate sensor and utilized to monitor phosphate ions in numerous urine samples [25]. Wang et al. utilized *in-situ* hydrothermally grown ZnO nanoflakes template to synthesize nanostructured cobalt electrodes for phosphate detection [26]. Ogabiela and Adeloju fabricated potentiometric based phosphate biosensor using entrapped pyruvate oxidase in a polypyrrole film [27]. Gavalas and Chaniotakis utilized physically adsorbed enzyme-polyelectrolyte complexes on the transducer to fabricate pyruvate oxidase-based phosphate biosensor [28]. However, most of approaches either used additive to attach nanostructures or time-taking and complex processes (i.e. polymerization) to deposit bioactive materials on the electrode surfaces. Therefore, simple and effective fabrication strategy is needed to fabricate low-cost and highly reproducible sensing electrodes with better sensing performances to overcome the significant challenges faced during sensing electrode fabrication using multiple steps.

Herein, we chose a simple low-temperature hydrothermal route to synthesize ZnO NRs array on the ZnO seeded area of $SiO_2$/Si substrates between silver source-drain electrodes. The vertically-grown ZnO NRs array offers larger surface area for pyruvate oxidase (PyO) immobilization and also serves as a channel for fast electron transport. Additionally, the direct growth of nanostructures is highly desirable for reproducibility and better sensing performance. To demonstrate the sensing performance of the proposed field-effect transistor (FET) biosensor, we measured phosphate concentrations in buffer solution which indicate a reliable application of fabricated FET biosensor for phosphate sensing.

## 2. Experimental details

### 2.1. Chemicals

Hexamethylenetetramine (HMTA; $C_6H_{12}N_4$, ≥99.0%), zinc nitrate hexahydrate ($Zn(NO_3)_2{\cdot}6H_2O$, 98%), pyruvate oxidase from *Aerococcus sp.* [EC 1.2.3.3; ≥35 units/mg protein (biuret)], potassium phosphate monobasic ($KH_2PO_4$, ≥99.0%), β-Nicotinamide adenine dinucleotide (NADH, ≥95%), $MgCl_2$, KCl, $CaCl_2$, $Na_2SO_4$, sodium pyruvate, thiamine pyrophosphate chloride (TPP), N-2-Hydroxyethylpiperazine-N′-2-ethanesulfonic acid (HEPES), and Nafion (5 wt%) were purchased from Sigma-Aldrich. 0.02 M HEPES buffer (pH 7.0) containing pyruvate, FAD, $Mg^{2+}$ and TPP was used a buffer medium, after maintaining the pH with 0.1 mM citrate buffer solution. All aqueous solutions were prepared using Milli-Q water purified deionized water.

### 2.2. Electrode preparation

In order to fabricate FET biosensor (Fig. 1), silver (Ag) source-drain electrode and ZnO seed layer were deposited in the unmasked regions of cleaned $SiO_2$/Si wafer by radio-frequency (RF) magnetron-sputtering using ZnO and Ag targets with 99.99% purity at 60 W RF power in two steps at room temperature. In step one, Ag source-drain (~100 nm) was deposited in a gas mixture of Ar and $N_2$ (each 25 sccm) at $2.6 \times 10^{-5}$ torr sputter chamber pressure. In the next step, ZnO seed layer (~60 nm) was sputter-deposited between pre-deposited Ag source-drain electrodes in Ar (25 sccm) atmosphere at $8.6 \times 10^{-5}$ torr (i). Then, ZnO NRs were grown on seeded area using our previous recipe [29]. In brief, 0.04 M of HMTA and 0.04 M $Zn(NO_3)_2{\cdot}6H_2O$ were dissolved in 50 mL deionized water and transferred into a Pyrex glass bottle, followed by heating in a laboratory oven for 4 h at 85 °C after suspending seeded substrates upside down (ii). After completion of reaction, electrodes were rinsed with deionized water to remove impurities. In the next step, ZnO NRs grown electrodes were rinsed with HEPES buffer before PyO immobilization. The stock solutions of enzyme were freshly prepared by dissolving PyO (7.0 U/mL) and NADH in ratio of 5:1 in HEPES buffer (0.02 M, pH 7.0). A 10 μL volume of above solution was immobilized on ZnO NRs surface for 12 h at 4 °C and then biosensor was briefly rinsed with HEPES buffer to remove un-immobilized PyO. Finally, 2 μL of 0.5 wt% Nafion solutions was dropped on electrode surface to protect enzyme leakage and enhance selectivity. Similarly, we prepared FET biosensors without growing ZnO NRs (bare FET biosensor) to compare and show the advantage of ZnO NRs.

### 2.3. Characterizations

The surface morphology of electrodes were characterized with field-emission scanning electron microscopy (FE-SEM, Hitachi S4700) after coating the samples with a thin layer (~7 nm) of Pt to avoid charging while taking images. To characterize the crystalline structure of ZnO NRs by transmission electron microscopy (TEM), vertically-grown ZnO NRs were carefully removed from substrate using the doctor-blade, followed by sonication in ethanol for 5 min, dip-coating on TEM grid, and drying TEM grid at 120 °C for 30 min. X-ray diffraction (XRD) was recorded using Cu-Kα radiation (λ = 1.54178 Å) by X-ray diffractometer (Rigaku) in the range of 30–60° with 8°/min scanning speed.

All the electrical characterizations were conducted using probe-station attached semiconductor parameter analyzer (Model: HP 4155A) at room temperature in ambient conditions. The source-drain electrodes of fabricated FET biosensors were passivated with PDMS before electrical measurements. For analyte detection, a

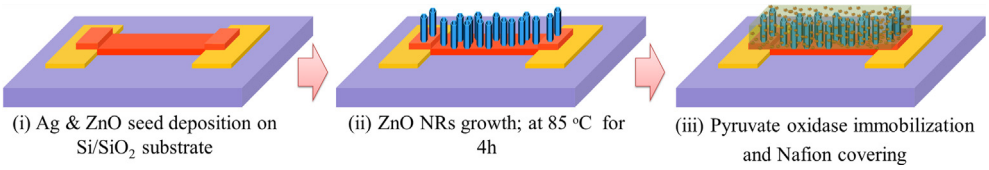


**Fig. 1.** Schematic showing FET biosensor fabrication process.

floating gate (Ag/AgCl) was utilized to measure the drain current with a fixed drain-source voltage of 0.1, while the gate-source voltage was increased in the range of 0–5.0 V. The different concentrations of analyte solutions (each 50 μL) were pipetted onto active area/channel area between source-drain electrodes and immediately electrical measurements were performed. For every measurement, the electrodes were rinsed in buffer prior to re-use. All experiments were performed in 0.02 M HEPES buffer containing sodium pyruvate.

## 3. Results and discussion

### 3.1. Characterization of ZnO NRs

Fig. 2 demonstrates top-view (a) and cross-sectional FESEM images (b) of as-synthesized ZnO NRs used for enzyme immobilizations. It can be seen from top-view image ZnO NRs were vertically aligned. The length of ZnO NRs is ~ 1.2 μm and thickness is estimated to be ~80–90 nm. After immobilization of PyO on ZnO NRs, it was hard to focus while taking FESEM images (Fig. 2c and d). This can be attributed to the enzyme coating on ZnO NRs. In Fig. 3a, the low-resolution TEM image of ZnO NRs exhibits smooth surface. The HR-TEM image clearly delineates fringes of ZnO planes along with interplanar spacing of ~0.52 nm (Fig. 3b). Together HR-TEM image and selected-area electron diffraction (SAED) pattern suggest that ZnO NR is grown along [0001] direction and possess wurtzite ZnO single crystal (Fig. 3c). The crystallinity and orientation of ZnO NRs were characterized by XRD (Fig. 3d). All observed peaks in pattern are well matched with bulk wurtzite ZnO (JCPDS Card No. 75-1526). A strong (0002) peak at 34.2° attributed to the preferred orientation of ZnO NRs, which is consistent with HRTEM and SAED results.

### 3.2. Current-voltage and electrocatalytic properties

The current-voltage ($I_D$-$V_D$) characteristics of ZnO NRs based FET was measured in the drain voltage ($V_D$) range of 0–15 V with increasing gate voltage ($V_G$) from 0 to 20 V (with 2 V step) at room temperature in ambient conditions. From Fig. 4, the FET shows typical n-type semiconductor behaviour. Additionally, we can clearly see a nice pinch-off and current saturation which follows the standard theory of FETs [30]. The electrocatalytic properties of as-fabricated FET biosensors (bare FET and with ZnO NRs based FET) were evaluated in a 0.02 M HEPES buffer without and with 0.10 mM phosphate (Fig. 5). Both FET biosensors showed no response in the absence of phosphate, however, a gradual current increase was noticed in the presence of phosphate. Bare FET biosensor showed poor current response compared to ZnO NRs based FET biosensor. The enhanced current response is due to the ZnO NRs which offers better surface area for enzyme immobilization. The PyO adsorbed on ZnO NRs surface catalyses reactions in phosphate solution and generate hydrogen peroxide ($H_2O_2$) and acetylphosphate according to the following reactions [31]:

$$\text{Pyruvate} + \text{Phosphate} + O_2 \rightarrow \text{Acetylphosphate} + H_2O_2 + CO_2 \quad (1)$$

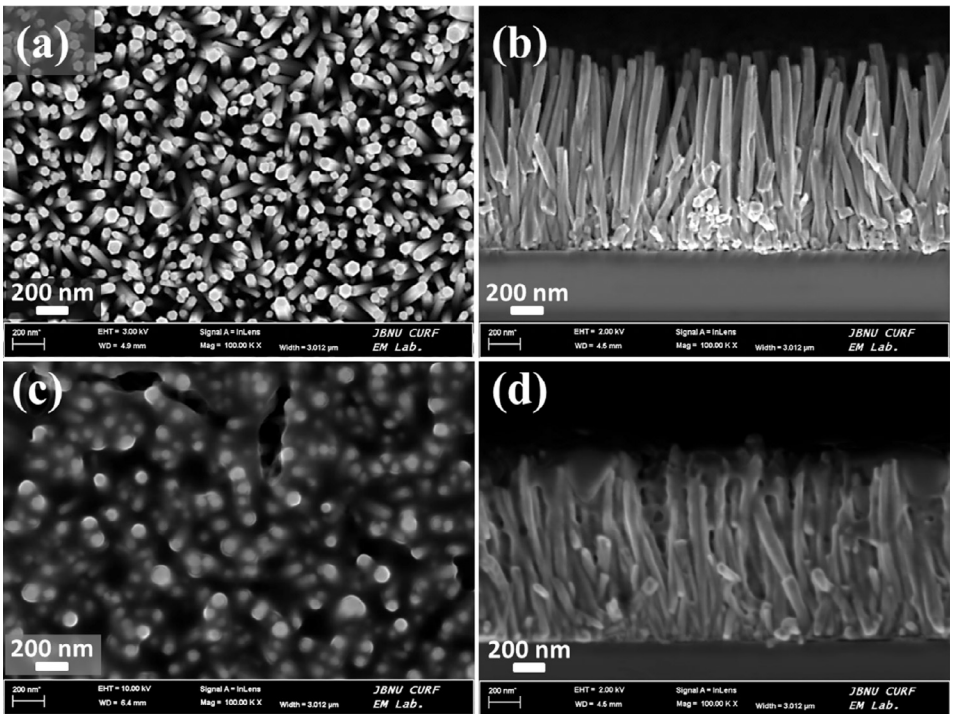


**Fig. 2.** Top-view and cross-sectional FESEM images of as-synthesized vertically aligned ZnO NRs (a & b) and PyO immobilized on ZnO NRs (c & d), respectively.

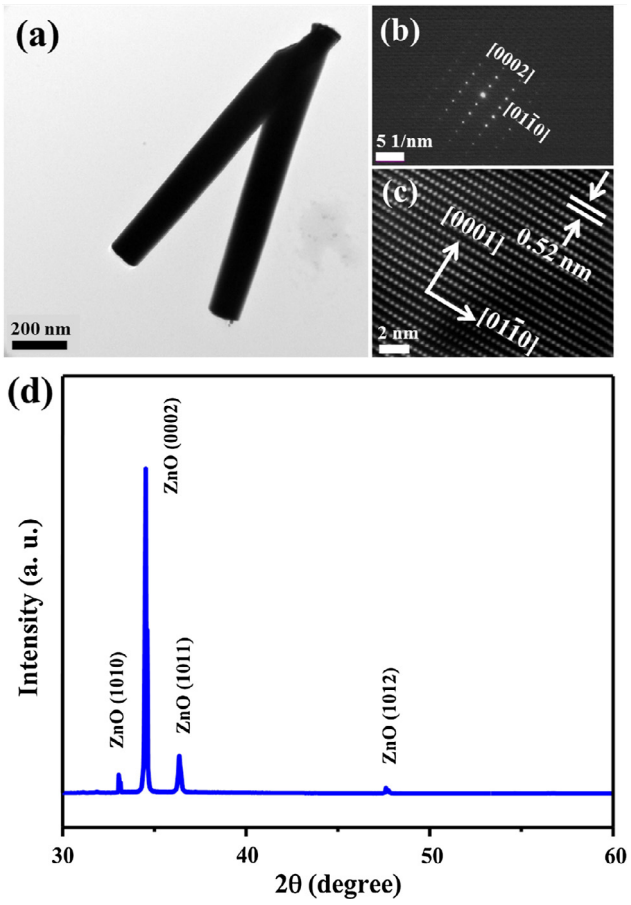


**Fig. 3.** Low-resolution TEM image of ZnO NRs (a) along with SAED pattern (b) and HR-TEM image (c). XRD pattern of ZnO NRs grown on $SiO_2$/Si at low temperature (d).

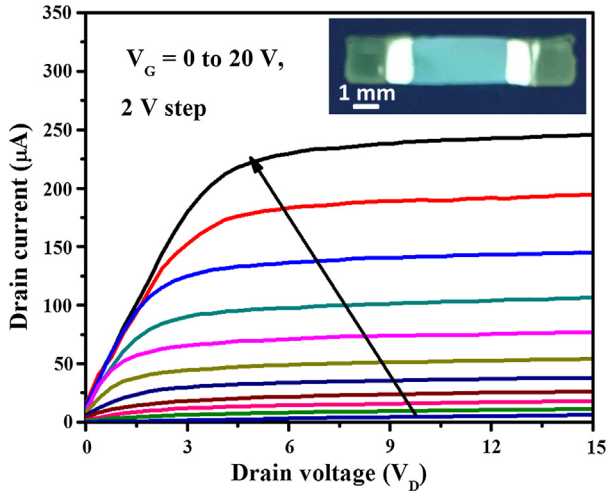


**Fig. 4.** Current-voltage ($I_D$-$V_D$) characteristics of ZnO NRs based FET in the drain voltage ($V_D$) range of 0–15 V with increasing gate voltage ($V_G$) from 0 to 20 V (with 2 V step) at room temperature in ambient conditions. Inset shows the optical image of FET.

$$H_2O_2 \rightarrow 2H^+ + 2e^- + O_2 \quad (2)$$

In the reaction (1) $H_2O_2$ is produced and then oxidized (2) to give sensing response during measurement. Therefore, the current response was increased after phosphate addition in HEPES buffer.

Next, we performed experiments to validate this phosphate detection method for quantification purposes. For this, we first

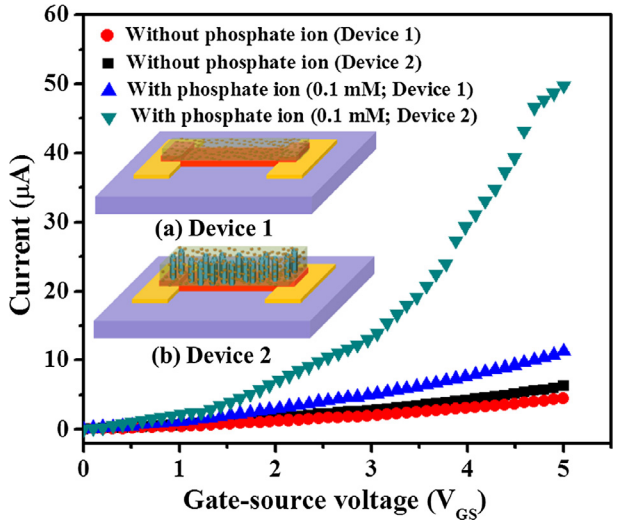


**Fig. 5.** *I-V* characterization of (a) bare FET (without ZnO NRs) and (b) ZnO NRs based FET biosensor in 0.02 M HEPES buffer (0.02 M, pH 7.0) without and with 0.10 mM phosphate. Insets show the bare FET (device 1) and ZnO NRs based FET (device 2) biosensors schematics.

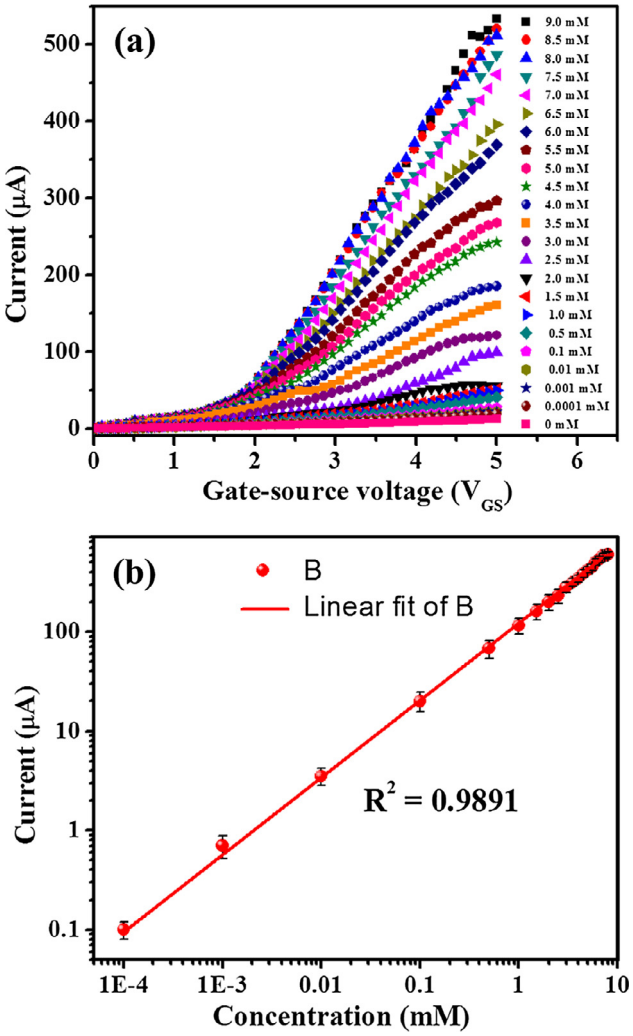


**Fig. 6.** (a) *I-V* characterization of FET biosensor with increasing phosphate concentrations from 0.1 μM to 9.0 mM in 0.02 M HEPES buffer (0.02 M, pH 7.0) and (b) their corresponding calibration curve *i.e.* response current *vs.* phosphate concentration (mM) in log scale.

**Table 1**
Comparison of our fabricated FET biosensor's sensing performances with recently reported phosphate biosensors.

| Electrode materials | Sensitivity | Linear range (μM) | Detection limit (μM) | Ref. |
|---|---|---|---|---|
| Carbon black printed paper | 0.115 μA/μM | 1–300 | 4 | [24] |
| Cobalt | −33.48 μA/decade | 10–100 | 10 | [26] |
| ZnO nanoflake-Cobalt | 13.17 μA/decade | 1–100 | 1 | [26] |
| Polypyrrole-PyO | 14.97 mV/decade | 15–400 | 3 | [27] |
| PyO-nano-particle comprised poly-5,2′:5′,2″-terthiophene-3′-carboxylic acid | 0.59 nA/μM | 1–100 | 0.3 | [31] |
| PyO-porous conductive carbon | 0.3 ± 0.2 μA/mM | 50–1250 | 4.8 | [32] |
| Cobalt | 33 mV/decade | 10–10,000 | 10 | [33] |
| PyO-ZnO NR | 80.57 μA/mM$^{-1}$ cm$^{-2}$ | 1–7000 | ~0.5 | This work |

prepared different concentrations of solutions containing $KH_2PO_4$ in HEPES buffer (0.02 M, pH 7.0). Then, *I-V* responses for phosphate were measured by applying solutions of phosphate with increasing concentrations (Fig. 6a). As shown in Fig. 6a, catalytic oxidation currents were observed to increase as the concentration of phosphate was increased. This confirms that our fabricated FET biosensor is capable to detection different concentrations of phosphate in solution. Each experiment was repeated three times and average of response currents was taken over a potentials range spanning of 2.0–5.0 V to draw the calibration plot (Fig. 6b). From plot presented in Fig. 6b, sensitivity of biosensor, linear detection range, and detection limit were determined. The FET biosensor showed linearity in a wide concentration range of phosphate (0.1 μM–7.0 mM) with high regression coefficients ($R^2$ = 0.9891) that indicates high accuracy in the assay range. Further, sensitivity (80.57 μA cm$^{-2}$ - mM$^{-1}$) was calculated from slope of current-concentration profile plots. The detection limit of phosphate was determined to be around ~50 nM. Table 1 shows the comparative result of our fabricated FET biosensor with recently reported phosphate biosensors. Compared with these reported sensing performances, our proposed FET biosensor has better sensitivity in wide linear range and low limit of detection [24,26,27,32]. The superior sensing performances of FET biosensor in the present study is mainly attributed to higher specific surface area of vertically grown ZnO NRs that immobilize higher amount of enzyme and also provides path for excellent electron transfer during electrocatalytic reactions [34,35]. Furthermore, ZnO NRs act as an eco-friendly support for immobilized enzyme that enhances the efficiency of enzyme and affinity between the enzyme and ZnO NRs support [36]. With these advantages, improved electrocatalytic activity of our FET biosensor was employed in monitoring phosphate.

### 3.3. Anti-interference, repeatability, stability, memory effect, and reproducibility tests

Anti-interference study of as-fabricated FET biosensor was investigated by detecting 0.5 mM phosphate with the addition of various interference species into HEPES buffer (0.02 M, pH 7.0). Fig. 7 shows the *I-V* response for different samples i.e. with and without interference species. Their calibrated responses are presented as histogram in inset of Fig. 7. From the calibrated histogram, detection of 0.5 mM phosphate showed no effect of low concentrations (0.1 mM) of each ion such as $K^+$, $SO_4^{2-}$, $Ca^{2+}$, $HCO_3^-$ and TPP. However, interfering species in higher concentration (0.5 mM) shows slight decrease in sensor response, suggesting fabricated biosensor exhibits high selectivity for phosphate detection. The obtained results can be attributed to the selectivity and specificity of immobilized PyO on the ZnO NRs surface.

The repeatability, stability and reproducibility of fabricated FET biosensor were also investigated. The current response was measured toward 0.5 mM phosphate for six repetitive experiments with same biosensor, which showed relative standard deviation (RSD) of ~4.3%. After 4 weeks storage under ambient condition,

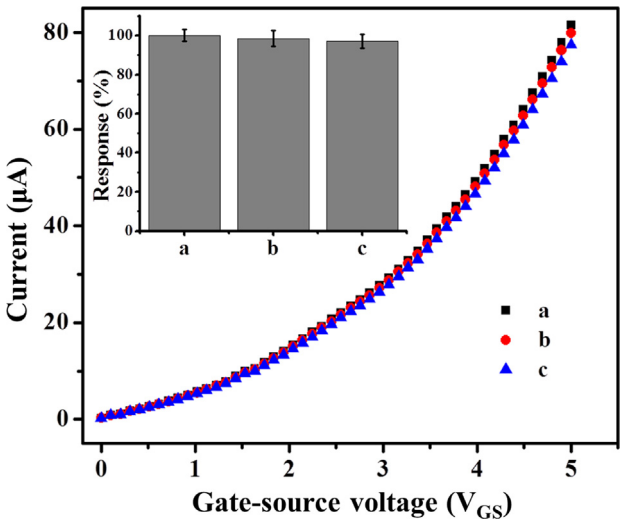


**Fig. 7.** Selectivity test showing *I-V* response of FET biosensor for 0.50 mM phosphate without any interfering species (a), and with 0.10 mM (b) and 0.50 mM each interfering species i.e. $K^+$, $SO_4^{2-}$, $Ca^{2+}$, TPP, and $HCO_3^-$ in 0.02 M HEPES buffer (0.02 M, pH 7.0). Inset histogram shows the calibrated responses.

the FET biosensor showed ~3.5% of current loss during 0.5 mM phosphate detection. However, there was no current decrease within the first week storage. Similar results were obtained for the detection of 0.5 mM phosphate with five independently fabricated FET biosensors. The obtained results strongly suggest that the fabricated biosensor possess high stability for repetitive detection of phosphate and are remarkably reproducible.

## 4. Conclusion

In summary, we have successfully fabricated phosphate FET biosensor based on ZnO NRs array grown on $SiO_2$/Si substrate after functionalization with PyO. The as-fabricated FET biosensor showed high sensitivity (80.57 μA mM$^{-1}$ cm$^{-2}$) in a wide-linear range (0.1 μM–7.0 mM), good selectivity, high stability and reproducibility. Encouraging results suggest that direct and vertically grown ZnO NRs provides high specific surface area for enhanced enzyme immobilization, which can lead to fabricate different biosensing electrodes with improved performances.

## Acknowledgements

This work was supported by the National Leading Research Laboratory program through the National Research Foundation (NRF) (NRF-2016R1A2B2016665) of Korea funded by the Ministry of Science, ICT & Future Planning. Authors also thank KBSI, Jeonju branch for SEM analysis and Mr. Jong-Gyun Kang, Center for University Research Facility (CURF) for taking good quality TEM images.

## References


[1] M.S. Razzaque, Phosphate toxicity: new insights into an old problem, Clin. Sci. (Lond) 120 (2011) 91–97.
[2] E. Ritz, K. Hahn, M. Ketteler, M.K. Kuhlmann, J. Mann, Phosphate additives in food – a health risk, Dtsch. Arztebl. Int. 109 (2012) 49–55.
[3] R.A. Sherman, O. Mehta, Phosphorus and potassium content of enhanced meat and poultry products: implications for patients who receive dialysis, Clin. J. Am. Soc. Nephrol. 4 (2009) 1370–1373.
[4] K. Kalantar-Zadeh, L. Gutekunst, R. Mehrotra, C.P. Kovesdy, R. Bross, C.S. Shinaberger, N. Noori, R. Hirschberg, D. Benner, A.R. Nissenson, J.D. Kopple, Understanding sources of dietary phosphorus in the treatment of patients with chronic kidney disease, CJASN 5 (2010) 519–530.
[5] Institute of Medicine. Dietary reference intakes for calcium, phosphorus, magnesium, vitamin D and fluoride. Prepared by the Standing Committee on the Scientific Evaluation of Dietary Reference Intakes, Food and Nutrition Board, Institute of Medicine. Washington, DC, USA, National Academy Press, 1997, pp. 190–249.
[6] D. Kaniansky, I. Zelensky, A. Hybenova, F.I. Onuska, Determination of chloride, nitrate, sulfate, nitrite, fluoride, and phosphate by on-line coupled capillary isotachophoresis-capillary zone electrophoresis with conductivity detection, Anal. Chem. 66 (1994) 4258–4264.
[7] C. Warwick, A. Guerreiro, A. Soares, Sensing and analysis of soluble phosphates in environmental samples: a review, Biosens. Bioelectron. 41 (2013) 1–11.
[8] S. Tobey, E. Anslyn, Determination of inorganic phosphate in serum and saliva using a synthetic receptor, Org. Lett. 5 (2003) 2029–2031.
[9] M. Ganjali, M. Hosseini, Z. Memari, F. Faridbod, P. Norouzi, H. Goldooz, A. Badiei, Selective recognition of monohydrogen phosphate by fluorescence enhancement of a new cerium complex, Anal. Chim. Acta 708 (2011) 107–110.
[10] H. Sun, A.M. Scharff-Poulsen, H. Gu, I. Jakobsen, J.M. Kossmann, W.B. Frommer, K. Almdal, Phosphate sensing by fluorescent reporter proteins embedded in polycrylamide nanoparticles, ACS Nano 2 (2008) 19–24.
[11] N. Modi, B. Patel, M. Patel, S. Menon, Novel monohydrogenphosphate ion-selective polymeric membrane sensor based on phenyl urea substituted calix [4]arene, Talanta 86 (2011) 121–127.
[12] F. Tafesse, M. Enemchukwu, Fabrication of a new solid state phosphate selective electrodes for environmental monitoring, Talanta 83 (2011) 1491–1495.
[13] S. Berchmans, R. Karthikeyan, S. Gupta, G. Poinern, T. Issa, P. Singh, Glassy carbon electrode modified with hybrid films containing inorganic molybdate anions trapped in organic matrices of chitosan and ionic liquid for the amperometric sensing of phosphate at neutral pH, Sens. Actuators B: Chem. 160 (2011) 1224–1231.
[14] W.-L. Cheng, J.-W. Sue, W.-C. Chen, J.-L. Chang, J.-M. Zen, Activated nickel platform for electrochemical sensing of phosphate, Anal. Chem. 82 (2010) 1157–1161.
[15] L.R. Adornato, E.A. Kaltenbacher, D.R. Greenhow, R.H. Byrne, High-resolution in situ analysis of nitrate and phosphate in the oligotrophic ocean, Environ. Sci. Technol. 41 (2007) 4045–4052.
[16] R. Vuillemin, D.L. Roux, P. Dorval, K. Bucas, J.P. Sudreau, M. Hamon, C.L. Gall, P. M. Sarradin, Chemini: a new in situ chemical miniaturized analyzer, Deep-Sea Res. Part I 56 (2009) 1391–1399.
[17] M. Han, D. Kim, Naked-eye detection of phosphate ions in water at physiological pH: a remarkably selective and easy-to-assemble colorimetric phosphate-sensing probe, Angew. Chem. Int. Ed. 41 (2002) 3809–3811.
[18] K. Niikura, A. Metzger, E. Anslyn, Chemosensor ensemble with selectivity for nositol-trisphosphate, J. Am. Chem. Soc. 120 (1998) 8533–8534.
[19] K. Johnson, C. Sakamoto-Arnold, C. Beehler, Continuous determination of nitrate concentrations in situ, Deep-Sea Res. Part A 36 (1989) 1407–1413.
[20] A. Daniel, D. Birot, S. Blain, P. Treguer, B. Leilde, E. Menut, A submersible flow-injection analyser for the in-situ determination of nitrite and nitrate in coastal waters, Mar. Chem. 51 (1995) 67–77.
[21] J.R. Clinch, P.J. Worsfold, An automated spectrophotometric field monitor for water quality parameters: determination of nitrate, Anal. Chim. Acta 200 (1987) 523–531.
[22] A.T. Lawal, S.B. Adeloju, Progress and recent advances in phosphate sensors: a review, Talanta 114 (2013) 191–203.
[23] V. Borse, P. Jain, M. Sadawana, R. Srivastava, 'Turn-on' fluorescence assay for inorganic phosphate sensing, Sens. Actuators B 225 (2016) 340–347.
[24] S. Cinti, D. Talarico, G. Palleschi, D. Moscone, F. Arduini, Novel reagentless paper-based screen-printed electrochemical sensor to detect phosphate, Anal. Chim. Acta 919 (2016) 78–84.
[25] A.A. Fadhel, M. Johnson, K. Trieu, E. Koculi, A.D. Campiglia, Selective nano-sensing approach for the determination of inorganic phosphate in human urine samples, Talanta 164 (2017) 209–215.
[26] X. Wang, X. Ma, J. Church, S. Jung, Y. Son, W.H. Lee, H.J. Cho, ZnO nanoflakes as a template for in-situ electrodeposition of nanostructured cobalt electrodes as amperometric phosphate sensors, Mater. Lett. 192 (2017) 107–110.
[27] E. Ogabiela, S.B. Adeloju, A potentiometric phosphate biosensor based on entrapment of pyruvate oxidase in a polypyrrole film, Anal. Methods 6 (2014) 5290–5297.
[28] V.G. Gavalas, N.A. Chaniotakis, Phosphate biosensor based on polyelectrolyte-stabilized pyruvate oxidase, Anal. Chim. Acta 427 (2001) 271–277.
[29] R. Ahmad, N. Tripathy, M.Y. Khan, K.S. Bhat, M.-S. Ahn, Y.-B. Hahn, Ammonium ion detection in solution using vertically grown ZnO nanorod based field-effect transistor, RSC Adv. 6 (2016) 54836–54840.
[30] Y.-K. Park, W.-Y. Rho, T. Mahmoudi, Y.-B. Hahn, Lateral growth of ZnO nanorod arrays in polyhedral structures for high on-current field-effect transistors, Chem. Commun. 50 (2014) 10502–10505.
[31] M.A. Rahman, D.-S. Park, S.-C. Chang, C.J. McNeil, Y.-B. Shim, The biosensor based on the pyruvate oxidase modified conducting polymer for phosphate ions determinations, Biosens. Bioelectron. 21 (2006) 1116–1124.
[32] V.G. Gavalas, N.A. Chaniotakis, Phosphate biosensor based on polyelectrolyte-stabilized pyruvate oxidase, Anal. Chim. Acta 427 (2000) 271–277.
[33] Z. Zou, J. Han, A. Jang, P.L. Bishop, C.H. Ahn, A disposable on-chip phosphate sensor with planar cobalt microelectrodes on polymer substrate, Biosens. Bioelectron. 22 (2007) 1902–1907.
[34] R. Ahmad, N. Tripathy, M.-S. Ahn, Y.-B. Hahn, Development of highly-stable binder-free chemical sensor electrodes for p-nitroaniline detection, J. Colloid Interface Sci. 494 (2017) 300–306.
[35] R. Ahmad, N. Tripathy, M.-S. Ahn, Y.-B. Hahn, Highly stable hydrazine chemical sensor based on vertically-aligned ZnO nanorods grown on electrode, J. Colloid Interface Sci. 494 (2017) 153–158.
[36] S. Datta, L.R. Christena, Y.R.S. Rajaram, Enzyme immobilization: an overview on techniques and support materials, 3 Biotech 3 (2013) 1–9.